1 **Title**

2 Human intestinal tissue-resident memory CD8+ T cells comprise transcriptionally

3 and functionally distinct subsets

4

5 **Authors (full names and institutions)**

6 Michael E.B. FitzPatrick[1]*, Nicholas M. Provine[1]*, Lucy C. Garner[1]*, Kate Powell[2], Ali

7 Amini[1], Sophie Irwin[1], Helen Ferry[1], Tim Ambrose[1,3], Peter Friend[3], Georgios Vrakas[3],

8 Srikanth Reddy[3], Elizabeth Soilleux[4], Paul Klenerman[1,2,5]†, Philip J. Allan[1,3,5]

9

10 *MF, NP, and LG contributed equally to this paper

11 †Corresponding author

12

13 1 Translational Gastroenterology Unit, Nuffield Department of Medicine, University of

14 Oxford, Oxford, UK

15 2 Peter Medawar Building for Pathogen Research, University of Oxford, UK

16 3 Oxford Transplant Centre, Oxford University Hospitals NHS Foundation Trust,

17 Churchill Hospital, Oxford, UK

18 4 Division of Cellular and Molecular Pathology, Addenbrooke's Hospital, Cambridge,

19 UK

20 5 NIHR Biomedical Research Centre, John Radcliffe Hospital, Oxford, UK

21

22

23

24      **Summary**

25      Heterogeneity within human tissue-resident memory T ($T_{RM}$) cells is poorly

26      understood. We show that transcriptionally, phenotypically, and functionally distinct

27      CD4+ and CD8+ $T_{RM}$ subsets exist in the human intestine, and that β2-integrin

28      expression identifies a distinct population of CD8+ $T_{RM}$ cells.

29

30      **Abstract**

31      Tissue-resident memory T ($T_{RM}$) cells provide key adaptive immune responses in

32      infection, cancer, and autoimmunity. However transcriptional heterogeneity of human

33      intestinal $T_{RM}$ cells remains undefined, and definitive markers of CD103- $T_{RM}$ cells are

34      lacking. Here, we investigated transcriptional and functional heterogeneity of human

35      $T_{RM}$ cells through the study of donor-derived intestinal $T_{RM}$ cells from intestinal

36      transplant recipients. Single-cell transcriptional profiling identified four conventional $T_{RM}$

37      populations, with two distinct transcriptional states of CD8+ $T_{RM}$ cells, delineated by

38      *ITGAE* and *ITGB2* expression. We defined a transcriptional signature discriminating the

39      two CD8+ populations, including differential expression of key residency-associated

40      genes and cytotoxic molecules. Flow cytometry of recipient-derived cells infiltrating the

41      graft and intestinal lymphocytes from healthy gut confirmed the two CD8+ $T_{RM}$

42      phenotypes, with β2-integrin acting as a CD103- CD8+ $T_{RM}$ marker. CD103+ CD8+ $T_{RM}$

43      cells produced IL-2, and demonstrated greater polyfunctional cytokine production, while

44      β2-integrin+ CD69+ CD103- $T_{RM}$ cells had higher granzyme expression. Phenotypic and

45      functional analysis of intestinal CD4+ T cells identified many parallels, including a

46      distinct β2-integrin+ population. Together, these results describe the transcriptional,

2

47    phenotypic, and functional heterogeneity of human intestinal $T_{RM}$ cells, and suggest a

48    role for β2-integrin in $T_{RM}$ development.

49

50    **Introduction**

51    Tissue-resident memory T ($T_{RM}$) cells are a subset of long-lived T cells that reside in

52    tissue and do not recirculate (Mackay and Kallies, 2017; Szabo et al., 2019). $T_{RM}$

53    populations provide rapid, *in situ* adaptive protection against a wide spectrum of

54    pathogens (Gebhardt et al., 2011; Schenkel et al., 2014). $T_{RM}$ cells also have key roles

55    in cancer immune surveillance (Park et al., 2019), and are implicated in autoimmunity,

56    including inflammatory bowel disease (IBD) and coeliac disease (Zundler et al., 2019;

57    Mayassi et al., 2019). CD8+ $T_{RM}$ cells have potent cytotoxic functions and produce pro-

58    inflammatory cytokines to trigger innate and adaptive immune responses (Ariotti et al.,

59    2014).

60

61    Murine work has advanced our understanding of $T_{RM}$ cells substantially, however

62    $T_{RM}$ phenotype, transcriptional profiles, and genetic regulation differ between mice and

63    humans (Oja et al., 2017; Hombrink et al., 2016; Kumar et al., 2017). Until recently,

64    human studies of $T_{RM}$ biology were hampered by the inability to prove long-lived tissue

65    residency, with surface molecules CD69 and CD103 (αE integrin) used as surrogate

66    $T_{RM}$ markers. These were used to identify the putative transcriptional signature of

67    human $T_{RM}$ cells, with CD69 hypothesised as the key residency marker (Kumar et al.,

68    2017). However, this gene signature was derived from bulk populations, so it remains

69    unclear if there are transcriptionally distinct subsets within human $T_{RM}$ cells.

3

70

71     Despite its expression on almost all murine and human $T_{RM}$ cells, the use of CD69

72     as a residency marker has recently been questioned. CD69 restricts lymphocyte tissue

73     egress via S1P1 inhibition, but is not required for the development of functional $T_{RM}$

74     cells in mice (Shiow et al., 2006; Walsh et al., 2019). CD69 can be induced via

75     stimulation, and a proportion of CD69+ T cells in tissue are not resident, making CD69 a

76     suboptimal residency marker (Shiow et al., 2006; Sancho et al., 2005; Beura et al.,

77     2018). Therefore, additional phenotypic markers to identify CD103- $T_{RM}$ populations are

78     required.

79

80     Recent work has exploited the human model of organ transplantation to study long-

81     lived donor-derived T cells, which are definitive functionally resident $T_{RM}$ cells (Zuber et

82     al., 2016; Bartolomé-Casado et al., 2019; Snyder et al., 2019). Studies using this

83     approach have demonstrated persistence of clonally-identical intestinal CD8+ $T_{RM}$ cells

84     for up to 1 year in the small intestine (SI) (Bartolomé-Casado et al., 2019), and of donor-

85     derived T cells for 600 days post-transplant (Zuber et al., 2016). This approach was also

86     used to identify putative SI CD8+ $T_{RM}$ cell subsets based on expression of CD103 and

87     KLRG1, with differences in clonality, granzyme expression, and cytokine production

88     (Bartolomé-Casado et al., 2019). However, it remains unclear whether these cell

89     populations represent transcriptionally distinct subsets.

90

91     This work sought to examine the heterogeneity within functionally resident donor-

92     derived T cells in intestinal transplantation using flow cytometry and single-cell RNA

4

93    sequencing (scRNAseq). We confirmed that SI CD4+ and CD8+ $T_{RM}$ cells can persist

94    for 5 years post-transplant. scRNAseq identified conventional and regulatory CD4+ $T_{RM}$

95    cell populations, as well as two transcriptionally distinct CD8+ $T_{RM}$ subsets, which

96    differed in expression of *ITGAE* (CD103, αE integrin) and *ITGB2* (CD18, β2-integrin).

97    These two populations differentially expressed putative $T_{RM}$-associated genes,

98    indicating that the gene signatures derived from bulk RNAseq data may be a synthesis

99    of several transcriptomic profiles. We validated this phenotypic and functional

100   heterogeneity in the healthy intestine, with increased β2-integrin expression and

101   distinctive effector function in CD103- $T_{RM}$ cells. CD69, β2-integrin, and CD103

102   expression altered with time post-transplant on recipient-derived graft-infiltrating CD8+ T

103   cell populations, consistent with acquisition of $T_{RM}$ status. We conclude that CD69+

104   CD103- β2-integrin+ CD8+ intestinal T cells are a transcriptionally and functionally

105   distinct $T_{RM}$ population, and suggest that β2-integrin can serve as a proxy surface

106   marker for the CD103- CD8+ $T_{RM}$ population.

107

108   **Results and discussion**

109

110   ***Long-lived conventional CD4+ and CD8+ T cells, but not innate-like***

111   ***populations, persist long-term in the human intestine***

112

113   To examine the persistence of resident T cells in the small intestine (SI) post-

114   transplant, we used HLA allele congenic cell tracking, a method allowing discrimination

115   of donor- and recipient-derived cells following transplantation using fluorophore-

116   conjugated antibodies to discordant Class I HLA haplotypes (Fig. 1A, Supplemental Fig.

117   1A) (Zuber et al., 2016; Bartolomé-Casado et al., 2019). The presence of SI donor- and

118   recipient-derived T cells *in situ* was confirmed by chip cytometry (Fig. 1B)(Leng et al.,

119   2019).

120

121       Infiltration of recipient-derived T cells into the graft increased over time, with striking

122   heterogeneity (Fig. 1C). Current or previous rejection was associated with higher

123   proportions of recipient-derived T cells in the graft (Fig. 1D), consistent with prior work

124   (Zuber et al., 2016). Conversely, two individuals had persistent donor-derived SI T cell

125   populations at 4 years 7 months (1684 days) and 5 years 1 month (1865 days) post-

126   transplant (Fig. 1E, and data not shown). This extends previous reports of long-lived

127   donor-chimerism in the human intestine (Zuber et al., 2016; Bartolomé-Casado et al.,

128   2019).

129

130       Haematopoietic stem and progenitor cells can persist in the intestinal transplant

131   graft, sometimes leading to long-term chimerism of donor-derived populations in blood

132   (Fu et al., 2019). This could allow persistence of donor-derived T cells in the graft

133   through continuous ingress from blood, rather than via residency (Bartolomé-Casado et

134   al., 2019). Contrasting with the work of Fu *et al.*, flow cytometric analysis of blood

135   collected from transplant recipients at the time of biopsy revealed the percentage of

136   circulating donor origin T cells was extremely low beyond 3 months post-transplant

137   (median 0.042%, 95% CI 0-1.22%; Fig. 1F). This is far below the posited cut-off for

138   macrochimerism of 4% in previous work (Fu et al., 2019), and similar to background

139    non-specific staining in non-transplant recipients (0.01-0.12%; Supplemental Fig. 1B),

140    suggesting against continuous replacement as a confounding mechanism for sustained

141    donor chimerism. This discrepancy in circulating chimerism between studies may be

142    due to differences in transplant procedure (multi-visceral vs isolated intestinal transplant

143    in this study) and recipient age (paediatric vs adult in this study) (Zuber et al., 2015; Fu

144    et al., 2019).

145

146       Conventional CD4+ and CD8+ T cells dominated in the graft post-transplant (Fig.

147    1G), and demonstrated similar kinetics of recipient-derived replacement with time (Fig.

148    1H). We also examined the dynamics of unconventional T cell subsets post-transplant,

149    as their residency characteristics in humans are poorly understood (Supplemental Fig.

150    1C). CD161+Vα7.2+CD8+ T cells (consistent with mucosal-associated invariant T

151    (MAIT) cells), and Vδ2+ γδ T cells (which possess analogous innate-like functions to

152    MAIT cells (Provine et al., 2018; Gutierrez-Arcelus et al., 2019)) were rare in the graft

153    post-transplant, recovering to expected frequencies after 1 year (Fig, 1I) . However, the

154    non-Vδ2 γδ T cell subsets demonstrated different dynamics, with this population present

155    at early timepoints. Unconventional T cell subsets demonstrated similar replacement

156    kinetics (Fig. 1J). It is unclear if the low innate-like T cell frequency post-transplant is

157    due to differences in residency characteristics, or to increased sensitivity to the

158    ischaemic insult of surgery or perioperative conditioning regimes.

159

160       We examined CD69 and CD103 expression on donor- and recipient-derived CD4+

161    and CD8+ T cell populations in the intestinal graft. CD103 expression was restricted to

162    CD69+ cells, with a greater proportion of CD8+ cells expressing CD103 than CD4+

163    cells(Fig. 1K), in keeping with prior work  (Kumar et al., 2017). Donor-derived T cells

164    showed near-ubiquitous expression of CD69 consistent with a lack of recent migration

165    from blood, and had fewer CD69- cells than recipient-derived populations for both CD8+

166    (median 0.03% vs 4.17%, p<0.0001, Wilcoxon signed rank test) and CD4+ cells

167    (median 0.10% vs 5.65%, p<0.0001, Wilcoxon signed rank test) (Fig. 1L). This suggests

168    that CD69- T cells in the SI are not functionally resident in humans, in contrast to recent

169    murine data which showed no functional requirement for CD69 to establish intestinal

170    residency (Walsh et al., 2019).  Recipient-derived CD4+ and CD8+ T cell populations

171    showed increasing expression of CD103 with time, consistent with the acquisition of a

172    $T_{RM}$ phenotype, as in prior work (Zuber et al., 2016). We have previously shown higher

173    expression of the C-type lectin-like receptor CD161 on intestinal CD103+ CD8+ T cells

174    (Fergusson et al., 2015); here a greater proportion of donor-derived CD8+ T cells

175    expressed CD161, consistent with an association with residency (Supplemental Fig.

176    1D,E).

177

178    ***Single-cell RNA sequencing delineates transcriptionally distinct states within***

179    ***CD4+ and CD8+ $T_{RM}$ populations***

180

181    The persistence of CD103- and CD103+ donor-derived T cells up to five years post-

182    transplant, and the enrichment of CD103+ recipient-derived T cells at later time points,

183    raised the possibility that CD103- and CD103+ T cells represented distinct cell states.

184    To test this hypothesis, we performed droplet-based scRNAseq of sorted donor-derived

185 graft-resident $T_{RM}$ cells from a single subject one year post-transplant (Experiment 1,

186 Fig. 2A). 1,774 cells were captured and sequenced, with 974 cells remaining after

187 filtering (Supplemental Fig. 2A).

188

189  Four transcriptionally distinct clusters were identified (Fig. 2B): conventional CD4+ T

190 cells, regulatory CD4+ T cells expressing *IL2RA* and *FOXP3*, and two clusters of

191 conventional CD8+ T cells (Fig. 2C). The differentially expressed genes (DEGs)

192 between the two populations of donor-derived CD8+ $T_{RM}$ cells (hereafter CD8+

193 population 1 and 2) were analysed (Fig. 2D). Population 1 expressed *ITGAE* (CD103),

194 as well as higher levels of *CD7*, *IL7R* (CD127), *KLRB1* (CD161), and the chemokine

195 receptor *CCR6* (Fig. 2E). IL-7, a stromal-derived homeostatic cytokine which provides

196 survival and proliferative signals to lymphocytes (Raeber et al., 2018), is required for

197 epidermal $T_{RM}$ persistence (Adachi et al., 2019), and *CD127* is highly expressed in SI

198 memory T cells (Thome et al., 2014). The differential expression of IL7R suggests

199 differences in the mechanisms, or nature, of $T_{RM}$ persistence between the two

200 populations (Raeber et al., 2018).

201

202  Conversely, CD8+ population 2 expressed low levels of *ITGAE*, but high levels of

203 *KLRG1*, as well as cytotoxic granzyme molecules and class II MHC molecules (Fig.

204 2D,E). Surface KLRG1 expression can delineate two putative SI CD103- CD8+ T cell

205 subsets with similar residency characteristics (Bartolomé-Casado et al., 2019).

206 However, population 2 did not sub-cluster further based on *KLRG1* gene expression,

207 suggesting that these are not transcriptionally distinct states. Of particular interest, the

208    integrin *ITGB2* (β2-integrin/CD18), was highly expressed by the CD103- CD8+

209    population 2. β2-integrin can form heterodimers with four α-integrins (Fagerholm et al.,

210    2019), only one of which, *ITGAL* (CD11a), was detected in the dataset. *ITGAL* was

211    highly expressed on the CD103- CD8+ population 2 (Supplemental Fig. 2B,C).

212

213    **CD8+ CD103+ and CD103-ITGB2hi T$_{RM}$ subsets differ in expression of putative**

214    **residency-associated genes**

215

216        Transcriptional signatures associated with human tissue residency have been

217    defined, most thoroughly by bulk RNA sequencing of CD69- and CD69+ T cells from

218    multiple tissues (Kumar et al., 2017). This T$_{RM}$ gene set was explored in the two CD8+ T

219    cell populations. The genes downregulated in CD69+ T cells were either not detected,

220    or found at low levels in both clusters (Supplemental Fig. 2D,E). However, several T$_{RM}$-

221    associated genes upregulated in CD69+ T cells were differentially expressed between

222    the two clusters, with population 1 expressing higher levels of *ITGAE* and *ITGA1* (in

223    agreement with work on renal T$_{RM}$ cells (de Leur et al., 2019)), and population 2

224    expressing higher levels of *CRTAM* (Fig. 2F, Supplemental Fig. 2F). In addition,

225    *ZNF683* (Hobit), a transcriptional regulator of residency in mice (Mackay et al., 2016),

226    was more highly expressed in population 1. These data indicate that previously

227    identified T$_{RM}$ gene signatures may represent an amalgamation of several distinct T$_{RM}$

228    transcriptional states.

229

230        To confirm the presence of transcriptionally distinct CD8+ T$_{RM}$ states, a second

10

231 scRNAseq experiment was performed on samples from two further transplant recipients

232 (Experiment 2, Fig. 2A). Donor-derived CD103- and CD103+ CD8+ T cells were index-

233 sorted before plate-based scRNAseq using the Smart-Seq2 protocol (Picelli et al.,

234 2013). 267 cells were sorted and sequenced, with 196 cells remaining post-filtering

235 (Supplemental Fig. 2G-I).  Three clusters were identified, with cluster 1 predominantly

236 formed of CD103- T cells, and the transcriptionally similar clusters 2 and 3 formed of

237 CD103+ T cells (Fig. 2G). Clusters 2 and 3 (CD103+) expressed higher levels of

238 *ITGAE*, *CD7*, and *IL7R*, while cluster 1 (CD103-) expressed higher levels of *GZMK*,

239 *GZMH*, class II HLA molecules, and *ITGB2* (Fig. 2H). *ITGAL*, was also detected in

240 cluster 1 (Supplemental Fig. 2J).

241

242     Differential expression analysis between cluster 1 and clusters 2 and 3 combined

243 revealed similar transcriptional differences to those in Experiment 1 (Fig. 2I,

244 Supplemental Table 2). Comparison of DEGs in the two experiments identified a core

245 set of 30 genes that distinguished the two populations (Fig. 2I,J).

246

247     Putative $T_{RM}$ cell subsets in the context of lung transplantation have been described,

248 however these did not align with CD103 expression (Snyder et al., 2019), in contrast to

249 our work. The transcriptional signatures of the clusters were also different in our work,

250 with the exception of *ZNF683*, which was also associated with one lung $T_{RM}$ subset.

251 These differences may reflect tissue-specific gene signatures in $T_{RM}$ cells, differences in

252 CD4+ and CD8+ $T_{RM}$ cells, which co-clustered in the previous study of lung $T_{RM}$ cells, or

253 may be an effect of increased cell number in this study, allowing greater power to detect

11

254    transcriptionally distinct sub-clusters.

255

256    ***CD103+ and CD103- CD8+ T cells display distinct phenotypes in the healthy***

257    ***intestine***

258

259    The presence of CD103- and CD103+ donor-derived CD8+ T cells in the

260    transplanted SI mucosa was confirmed using chip cytometry (Fig. 3A). Flow cytometry

261    of donor-derived T cells demonstrated differences in expression of CD161, β2 integrin,

262    and granzyme K between CD103- and CD103+ CD8+ T cells, consistent with

263    scRNAseq data (Supplementary Fig. 3A).

264

265    To validate the phenotypic differences between the two putative SI CD8+ $T_{RM}$

266    subsets outside the transplant setting, we performed flow cytometry of SI T cells from

267    healthy donors. CD8+ SI T cells expressing both CD69 and CD103 predominated,

268    representing 88.9% (81.7-96.0%) of CD8+ T cells, with no difference seen between SI

269    location (Supplementary Fig. 3B).

270

271    CD103+ CD8+ T cells expressed higher levels of CD161 and CD127 (IL7R)

272    compared with the CD69- or CD69+CD103- cells, consistent with the transcriptomic

273    data (Fig. 3B,C). CD7 expression was higher on all CD69+ T cells, with no difference

274    seen between CD69+CD103- and CD69+CD103+ populations. In contrast,

275    CD69+CD103- CD8+ T cells expressed higher levels of β2-integrin, granzyme K, and

276    KLRG1 than either CD69- cells or CD69+CD103+ cells.

277

278      Ki-67 expression formed a gradient between the three populations, with higher

279    expression in the CD69- population, and a trend towards increased Ki67 expression in

280    CD69+CD103- CD8+ T cells compared to CD103+ CD8+ T cells (mean 14.88% vs

281    5.72%, 1-way ANOVA and Tukey's multiple comparisons test, P=0.067). This is

282    consistent with prior work indicating that $T_{RM}$ cell persistence is due to longevity rather

283    than *in situ* proliferation (Thome et al., 2014).

284

285    ***Graft-infiltrating, recipient-derived T cells take on a $T_{RM}$ phenotype over time,***

286    ***with CD103+ and CD103- CD8+ T cells displaying distinct phenotypes***

287

288      To explore the dynamics of $T_{RM}$ phenotype acquisition, we examined graft-

289    infiltrating, recipient-derived T cells. In the early post-transplant period, 52.7% of

290    infiltrating CD8+ T cells lacked CD69 expression, with acquisition of the CD69+ CD103+

291    $T_{RM}$ phenotype over time (Fig. 3D). At later times post-transplant, CD103- and CD103+

292    populations clearly differed in phenotype, consistent with the two subsets seen in

293    healthy SI. CD161 expression was higher on CD103+ CD8+ T cells than CD69+CD103-

294    T cells, and granzyme K expression was higher on CD69+CD103- CD8+ T cells (Fig.

295    3E-H). A similar gradient of Ki-67 expression between the populations was seen (Fig.

296    3F). In addition, graft-infiltrating CD69+CD103- CD8+ T cells demonstrated higher

297    expression of β2 integrin than either CD69- or CD103+ populations (Fig. 3I). β2 integrin

298    expression is constitutively high on circulating T cells (Fig. 3J), as LFA-1 is involved in

299    tissue entry via ICAM-1 (Fagerholm et al., 2019). These data suggest that β2 integrin

300     surface expression is reduced on recent tissue immigrants, before subsequent up

301     regulation on CD69+CD103- $T_{RM}$ cells, but not on CD103+ $T_{RM}$ cells. Recipient-derived

302     CD8+ T cells infiltrating the graft in the early post-transplant period displayed less clear

303     distinctions between populations, although the small number of samples precluded

304     further analysis.

305

306     ***CD103+ CD8+ intestinal T cells demonstrate greater capacity for cytokine***

307     ***production***

308

309     To assess cytokine production capacity of these subsets, SI T cells from healthy

310     controls were stimulated for four hours with PMA+ionomycin, before intracellular flow

311     cytometry for TNFα, IFNγ, IL-2, CCL4, IL-17A, and IL-10. 77% of CD103+ CD8+ T cells

312     produced at least one cytokine, a greater proportion than CD69+CD103- CD8+ T cells

313     (47.7% cytokine positive, P<0.0001), and CD69- CD8+ T cells (37% cytokine positive,

314     P<0.0001) (Fig. 4A-F). CD69+ populations produced more TNFα and IFNγ than CD69-

315     cells, irrespective of CD103 expression (Fig. 4A,B). While scRNAseq data indicated

316     increased *CCL4* transcripts in CD69+CD103- CD8+ T cells, CCL4 production following

317     stimulation was not different between the two CD69+ populations (Fig. 4C).

318

319     CD103+ CD8+ T cells expressed more IL-2 than either CD69+CD103- or CD69-

320     populations (Fig. 4D). Hepatic CD103+ CD8+ $T_{RM}$ cells also produce increased IL-2

321     (Pallett et al., 2017). Autocrine IL-2 production is critical to secondary proliferative

322     responses and IFNγ production in CD8+ T cells (Feau et al., 2011), and may be of

14

323 particular relevance to intra-epithelial lymphocyte populations, where the infrequent

324 CD4+ T cells may provide suboptimal help (Zimmerli et al., 2005).

325

326  There was a spectrum of functionality between the three populations, with CD69-

327 CD8+ T cells predominantly non- or mono-functional, CD103+ CD8+ T cells

328 predominantly polyfunctional, and CD69+CD103- CD8+ T cells showing intermediate

329 functionality (Fig. 4E,F), consistent with a prior report (Bartolomé-Casado et al., 2019).

330 Quadruple functional cells were more common in the CD103+ population than in the

331 CD69+CD103- population (21.76% vs 10.32%, P<0.0001), and were near-absent in the

332 CD69- population (0.38%). These results demonstrate that the transcriptionally distinct

333 CD103- and CD103+ CD8+ $T_{RM}$ populations differ functionally and phenotypically, with

334 CD103+ CD8+ populations more polyfunctional, and producing IL-2.

335

336 ***CD103+ and CD103- CD4+ T cells display analogous phenotypic and functional***

337 ***differences to their CD8+ counterparts***

338

339  Despite not forming transcriptionally distinct clusters by scRNAseq, CD4+ SI T cells

340 differed in their phenotype, dependent on CD69 and CD103 expression. CD69-

341 populations expressed lower levels of CD161 and CD127, while CD69+CD103- CD4+ T

342 cells had higher expression of β2-integrin than either CD69- or CD103+ populations,

343 analogous to their CD8+ counterparts (Fig. 5A). Recipient-derived, graft-infiltrating

344 CD69+CD103- CD4+ T cells also displayed higher expression of β2-integrin than

345 CD103+ counterparts (MFI 51,753 vs 30,959, P<0.0001; Fig. 5B).

346

347    A donor-derived regulatory CD4+ FOXP3+ population was detected in the

348    scRNAseq data (Fig. 2C), and donor-derived CD25+CD127- CD4+ T cells were

349    detected by flow cytometry in some subjects, consistent with potential long-term

350    residency of SI CD4+ regulatory T cells (Supplementary Fig. 3C). Low cell number of

351    this population precluded further analysis.

352

353    CD69+ CD4+ SI T cells showed higher production of multiple cytokines upon short-

354    term stimulation compared with CD69- T cells (Fig. 5C-I). In particular, IL-17A

355    production was almost exclusively restricted to CD69+ T cells (Fig. 5C). CD103+ CD4+

356    T cells demonstrated higher production of TNFα, CCL4, IL-17A, and IL-10 than CD69+

357    CD103- counterparts. There was a similar gradient of functionality between the three

358    CD4+ populations, with CD103+ cells showed greatest polyfunctional cytokine

359    production (Fig. 5I), as seen in CD8+ T cells. In summary, CD4+ SI T cell populations

360    demonstrated analogous differences in phenotype and functionality to their CD8+

361    counterparts.

362

363    ***Discussion***

364

365    This study has identified two transcriptionally distinct states of functionally-resident

366    *bona fide* human intestinal CD8+ T$_{RM}$ cells, which differ in phenotype and cytokine

367    production. This was demonstrated using the rigorous approach of identifying donor-

368    derived populations in the intestinal graft post-transplant, which confirms functional

16

369    tissue residency. These data were replicated both within graft-infiltrating T cell

370    populations establishing residency *de novo*, and in the healthy gut. The CD8+ $T_{RM}$

371    subsets differ in the expression of several genes previously associated with the human

372    $T_{RM}$ signature, which suggests that these signatures, derived from bulk RNAseq data,

373    may represent an amalgam of transcriptionally distinct $T_{RM}$ subsets (Kumar et al., 2017).

374

375    The two identified CD8+ $T_{RM}$ populations differ in IL7R (CD127) expression, and in

376    IL-2 production, which may indicate differing persistence and proliferation properties, as

377    well as in the expression of chemokine receptors and integrins, indicating potential

378    differences in tissue homing and retention. Of particular interest, β2-integrin is more

379    highly expressed on CD69+CD103- $T_{RM}$ cells, a population which remains difficult to

380    positively distinguish from recent immigrants from the circulation. β2-integrin could, in

381    addition to CD69, represent an important positive marker to identify this population.

382

383    β2-integrin forms part of the heterodimer LFA-1, which facilitates firm adhesion on

384    blood vessel endothelium via ICAM-1, a critical stage in lymphocyte trafficking

385    (Fagerholm et al., 2019). β2-integrin also regulates the immunological synapse

386    providing a co-stimulatory signal, both in the interaction with antigen-presenting cells,

387    and with infected target cells (Liu et al., 2009). LFA-1 is up-regulated on liver-resident T

388    cells and facilitates their patrolling of hepatic sinusoids, indicating a role for LFA-1 in

389    $T_{RM}$ motility and tissue surveillance (McNamara et al., 2017). Intriguingly, the interaction

390    of LFA-1 with ICAM-1 reduces cellular responses to TGFβ, a key cytokine in $T_{RM}$

391    development (Verma et al., 2012), while TGFβ can inhibit LFA-1 expression and

17

392    function (Boutet et al., 2016). This suggests a role for β2-integrin in the development of

393    CD103- CD8+ $T_{RM}$ cells, which may be TGFβ-independent, as in mice (Bergsbaken and

394    Bevan, 2015).

395

396        The *ITGB2* locus is a differentially methylated region in the blood and mucosa in

397    IBD, and mucosal gene expression is associated with disease activity (Kennedy et al.,

398    2016; Harris et al., 2014; Román et al., 2013). We hypothesize that this association with

399    IBD, in which $T_{RM}$ cells play a key role (Zundler et al., 2019), could be mediated via

400    altered β2-integrin expression and its effects on $T_{RM}$ cells, or suggest a pathogenic role

401    for one of the two $T_{RM}$ subsets.

402

403        Single-cell transcriptional heterogeneity has previously been examined in lung $T_{RM}$

404    cells, with two potential subsets identified, characterised by predominantly different

405    gene signatures to those in our study (Snyder et al., 2019). However, their putative

406    subsets contained both CD4+ and CD8+ cells co-clustering, which separated clearly in

407    our study. $T_{RM}$ cell phenotype and behaviour in lung and intestine differ substantially,

408    and this finding may be driven by such tissue-specific differences, or be an effect of the

409    higher cell number in our study (Thome et al., 2014). It remains unclear if analogous

410    subsets to the intestinal populations described in this study exist in other tissues,

411    whether such subsets differ in residency characteristics and functional capacity, and

412    whether they play distinct roles in human health and disease.

413

414      In conclusion, we have used the human model of intestinal transplantation to study

415    single-cell heterogeneity in the donor-derived *bona fide* $T_{RM}$ intestinal T cells. We found

416    that CD8+ $T_{RM}$ cells form two transcriptionally, phenotypically, and functionally distinct

417    subsets, with parallel findings in CD4+ T cells. In particular, we report the association

418    between β2-integrin and CD69+CD103- intestinal $T_{RM}$ cells, which may prove not only a

419    useful marker for this population, but could also have a role in $T_{RM}$ development and

420    function.

421

422

423

424

425

426

427

428

429

430

431

432

433

434

435

436

437

438    **Materials and methods**

439

440    ***Human biological material***

441    Intestinal transplant recipients were identified via the Oxford University Hospitals

442    NHS Foundation Trust (OUHFT) transplantation service (Oxford, United Kingdom).

443    Healthy control study subjects were identified via the OUHFT endoscopy service at the

444    time of routine endoscopy. Peripheral blood and intestinal biopsies were taken at the

445    time of endoscopy under the study framework and consent of the Oxford

446    Gastrointestinal Illnesses Biobank (REC Ref: 16/YH/0247). Patient and sample

447    characteristics are described in Supplementary Table 1.

448    Small intestinal biopsies were collected at the time of endoscopy and transported in

449    R10 (RPMI-1640 [Lonza] + 10% FCS [Sigma-Aldrich] + 1% penicillin/streptomycin

450    [Sigma-Aldrich]), before cryopreservation in freezing medium (10% DMSO [Sigma-

451    Aldrich], 90% FCS [Sigma-Aldrich]). This method preserves immune cell viability,

452    surface marker expression, and function (Konnikova et al., 2018). When required,

453    samples were rapidly thawed in a 37$^{o}$C water bath, washed in 20ml R10 before tissue

454    dissociation.

455    Duodenal samples were incubated in R10 media with 1mg/ml Collagenase D

456    (Roche) and 100µg/ml DNase (Thermo Fisher Scientific) for one hour in a shaking

457    incubator at 37$^{o}$C. Biopsies were then dissociated by vigorous agitation using a

458    GentleMACS Dissociator (Miltenyi Biotec), then strained through a 70µm filter. Cells

459    were washed with R10 media. For samples undergoing *ex vivo* stimulation or cell

460    sorting, the mononuclear cells were isolated on a discontinuous 70% and 35% Percoll

20

461    gradient (GE Healthcare) by centrifugation at 700g for 20 minutes without brake.

462    Mononuclear cells were collected from the interface and washed in R10.

463    For multiplex fluorescence chip cytometry, single intestinal biopsies were embedded

464    in OCT cryo-embedding matrix (Thermo Fisher Scientific) then frozen in isopentane

465    (Sigma-Aldrich) suspended over liquid nitrogen, and stored at $-80^{o}$C until use.

466    Peripheral blood mononuclear cells (PBMCs) were isolated from subject blood

467    samples by density gradient centrifugation. In brief, blood was diluted 1:1 with PBS,

468    then layered onto Lymphoprep (Axis-Shield), and centrifuged at 973g for 30 minutes

469    without brake. The mononuclear layer was collected and washed with R10. Any

470    remaining red blood cells were lysed with ACK (Ammonium-Chloride-Potassium)

471    solution for 2-3 minutes, and washed again in R10, before cryopreservation in freezing

472    medium as above.

473

474    ***Ex vivo* stimulation**

475

476    *Ex vivo* stimulation was performed as previously described (Provine et al., 2018). In

477    brief, purified intestine-derived mononuclear cells were plated at approximately

478    $1x10^{6}$/well in a U-bottom 96-well plate. Cell stimulation cocktail containing phorbol 12-

479    myristate 13-acetate (PMA) and ionomycin (Biolegend) was added in accordance with

480    manufacturer's instructions in the presence of brefeldin A and monensin ( both

481    Biolegend). Cells were incubated at $37^{o}$C, 5% $CO_2$, for 4 hours.

482

483    ***Flow cytometry and cell sorting***

484

485      For surface marker staining, cells were stained in 50µL of FACS buffer (PBS + 1mM

486    EDTA + 0.05% BSA) for 30 minutes at $4^oC$. Surface antibodies and clones used were:

487    CD3 (OKT3 or UCHT1), Vδ2 (B6), CD4 (OKT4 or SK3), Vα7.2 (3C10), CD38 (HIT2),

488    CD103 (Ber-ACT8), γδTCR (11F2), CD69 (FN50), HLA-A2 (BB7.2), HLA-A3 (GAP.A3),

489    CD8 (SK1 or RPA-T8), CD161 (191B8), nearIR and zombie yellow fixable viability dye

490    (Thermo Fisher Scientific or Biolegend), β2 integrin/CD18 (L130), CD25 (2A3), KLRG1

491    (REA261), CD127 (A019D5), CD7 (M-T701).

492      For intracellular cytokine staining, after surface staining as above, cells were fixed

493    and permeabilised in 100µL Cytofix/Cytoperm solution for 20 minutes at $4^oC$ (BD

494    Biosciences). Cells were then washed twice in Perm/Wash buffer (BD Biosciences).

495    Intracellular staining was performed in 50µl of Perm/Wash buffer (BD Biosciences) for

496    30 minutes at $4^oC$ using the following antibodies and clones: CCL4 (D21-1351), Ki67

497    (B56), TNFα (MAb11, IL-17A (BL168), IFNγ (B27), IL-2 (MQ1-17H12), GzmK

498    (GM26E7), IL-10 (JES3-9D7).

499      After staining, cells were stored at $4^oC$ protected from light until data acquisition.

500    Flow cytometry data were acquired on a BD LSRII flow cytometer (BD BioSciences) or

501    Aurora spectral flow cytometer (Cytek). For fluorescence-activated cell sorting (FACS)

502    samples were surface stained as above, with DAPI (Thermo Fisher Scientific) used as

503    viability dye. FACS was performed on an AriaIII (BD Biosciences; 70µm nozzle).

504    Antibodies were purchased from BioLegend, BD Biosciences, Miltenyi Biotec, or

505    Thermo Fisher Scientific.

506

507 ***Flow cytometry data analysis and statistics***

508    Flow cytometry data were analysed using FlowJo version 9.9.5 and version 10.6.1

509 (FlowJo, LLC). Statistical analyses of flow cytometric data were performed using Prism

510 version 8 (Graphpad Software). For phenotypic analysis of rare cell subsets,

511 populations with fewer than 10 cells were excluded.

512

513 ***Chip cytometry***

514    Samples were frozen in OCT (as described above), cryosectioned onto coverslips

515 and placed in cytometer chips (Zellsafe Tissue chips, Zellkraftwerk, GmbH, Deutscher

516 Platz 5c, 04103 Leipzig, Germany). Sections were fixed *in situ* at room temperature for

517 10 minutes using 4% paraformaldehyde, then washed with 10 mL of PBS. Non-specific

518 binding was blocked by incubating in 5% goat serum (Thermo Fisher Scientific) in PBS

519 for 1 hour at room temperature. Fluorophore-conjugated antibodies (as above, plus pan-

520 cytokeratin (C-11, GeneTex), and Histone-H3 (17H2L9, Thermo Fisher Scientific)) were

521 diluted for staining in PBS. Immunostaining was performed iteratively, with up to three

522 colours applied simultaneously. Fluorophores were then bleached and additional

523 antibodies applied to build up the panel (Hennig et al., 2009). Images were acquired

524 using a Zellscanner One Chip cytometer (Zellkraftwerk) and ZellExplorer software.

525

526 ***10x Genomics library preparation and sequencing***

527

528    scRNAseq libraries were generated using 10x Genomics Chromium Single Cell

529 V(D)J Reagents Kits (v1 Chemistry) following manufacturer's instructions.  Cells were

530    resuspended in PBS with 0.04% BSA at ~1000 cells/µL and loaded onto a single lane of

531    the Chromium Controller.  Captured cell number was 1,774.  Library quality and

532    concentration was determined using a TapeStation (Agilent) and Qubit 2.0 Fluorometer

533    (Thermo Fisher Scientific).  Libraries were sequenced on an Illumina HiSeq 4000 as per

534    manufacturer's instructions to a mean depth of 63,471 mean reads/cell.  Library

535    generation and sequencing were performed at the Oxford Genomics Centre (Wellcome

536    Centre for Human Genetics, University of Oxford).

537

538    ***Smart-Seq2 library preparation and sequencing***

539

540    Single cells were index-sorted into 96-well plates with one cell per well in 2.3 µl lysis

541    buffer (0.8% (vol/vol) Triton X-100 and 2 U/µL RNase inhibitor). Smart-Seq2 libraries

542    were generated following the published protocol with External RNA Controls Consortium

543    (ERCC) RNA (1:100,000) added prior to sequencing (Picelli et al., 2014). cDNA was

544    pre-amplified by PCR (21 cycles). Libraries were sequenced on an Illumina HiSeq4000

545    with 75bp paired-end reads.  Library generation and sequencing were performed at the

546    Oxford Genomics Centre (Wellcome Centre for Human Genetics, University of Oxford).

547

548    ***Droplet-based (10x Genomics) scRNAseq data analysis***

549

550    FastQ generation, read alignment, barcode counting and UMI counting were

551    performed using the Cell Ranger pipeline v2.2.0.  Downstream processing steps were

552    performed using Seurat v2.3.4 (Butler et al., 2018; Stuart et al., 2019).  Briefly, TCR and

553     BCR genes, and genes expressed in fewer than 10 cells, were removed.  Cells with <

554     3460 UMIs (local minimum of the UMI distribution to the left of the mode UMI count), <

555     500 genes, and > 10,000 UMIs, > 2500 genes, and/or > 10% mitochondrial reads were

556     removed (Supplementary Fig. 2A).  Variable genes were identified using M3Drop

557     (Andrews et al., 2018).  Data were log normalised and scaled, with cell-cell variation

558     due to UMI counts, percent mitochondrial reads, and S and G2M cell cycle scores

559     regressed out.  The top 10 principal components (PCs) were used as input for graph-

560     based clustering (0.4 resolution), as determined by visual inspection of the scree plot.

561     Clusters were visualised by tSNE.  Differential gene expression analysis between

562     clusters was performed using the Wilcoxon Rank Sum test (FindMarkers function with

563     default parameters).

564

565     ***Plate-based (Smart-Seq2) scRNAseq data analysis***

566

567     Reads were trimmed to remove contaminating adapter and oligo-dT primer

568     sequences using Trimmomatic v0.36 (Bolger et al., 2014).  Trimmed reads were aligned

569     to the human genome (hg38 assembly) plus added ERCC "spike-in" sequences using

570     STAR v2.5.3a (--outFilterMismatchNoverLmax 0.04 --outFilterType BySJout --

571     outMultimapperOrder Random) (Dobin et al., 2012).  Alignments were filtered using

572     Samtools v1.6 (Li et al., 2009) to retain only primary alignments and properly paired

573     reads.  Ensembl gene counts were generated using featureCounts v1.6.0 (-C -B -p)

574     (Liao et al., 2014).  Poor quality cells that fit one or more of the following criteria were

575     removed from the analysis (Supplementary Fig. 2G-I): small log-library size (< 3 median

576    absolute deviations (MADs) below the median), low percentage of uniquely mapped

577    reads (< 55%), low gene count (< 3 MADs below the median), high percentage of

578    ERCCs (> 37.5%), or high mitochondrial read fraction (> 6%).  Outlier cells with a large

579    library size or high gene count (potential doublets) were also removed.  Genes with

580    "undetectable" expression were removed (gene defined as "detectable" if at least 5 read

581    counts in two cells), along with TCR (and BCR) genes.  Log normalised expression

582    values were generated using the normalize function from scater v1.10.1 (McCarthy et

583    al., 2017) with cell-specific size factors calculated using scran v1.12.1 (Lun et al., 2016).

584    Feature selection was performed using M3Drop v3.10.4 (FDR < 0.01) (Andrews et al.,

585    2018) and the expression matrix subset to retain only the selected genes.  Clustering

586    analysis was performed using SC3 v1.12.0 (Kiselev et al., 2017).  Clusters were

587    visualised by UMAP generated using the top 30 PCs (McInnes et al., 2018) (generated

588    using the top 30 principal components).  Differential gene expression analysis was

589    performed using DEsingle v1.2.1 (Miao et al., 2018) (FDR < 0.05).

590

591    Upon publication, data will be deposited in the NIH GEO database.

592

593    ***Supplemental material:***

594    • Supplemental Figure 1

595    • Supplemental Figure 2

596    • Supplemental Figure 3

597    • Table 1: Subject and sample characteristics

598    • Table 2: Differentially expressed gene list

599

**Author contribution**

601    MF, NP, LG, PK, and PA conceived and designed the study. Patient identification,

602    consent, and sample collection was performed by MF, TA, PF, GV, SR, and PA.

603    Experiments and analyses were performed by MF, NP, LG, KP, AA, SI, and HF. Cell

604    sorting was performed by HF. MF, NP, and LG created the figures. MF drafted the

605    article. MF, NP, LG, KP, AA, SI, HF, TA, PF, GV, SR, ES, PK, and PA critically revised

606    the article and approved the final version.

607

622

623    Figure 1. **Conventional T cell subsets persist for 5 years post-transplant, and**

624    **display a characteristic tissue resident memory ($T_{RM}$) phenotype.**

625    (A) Representative flow cytometry plot of HLA-A2 expression of T cells from the

626    blood, the recipient native intestinal mucosa, and the intestinal transplant graft,

627    demonstrating identification of donor- and recipient-derived populations by HLA

628    mismatch.

629    (B) Representative chip cytometry image of intestinal graft mucosa demonstrating

630    presence of donor-derived (HLA-A2+, yellow arrows) and recipient-derived (HLA-A2-,

631    white arrows) CD3+ T cells in the lamina propria. Cytokeratin (grey); CD3 (purple); HLA-

632    A2 (green).

633    (C) Percentage of recipient-origin CD3+ T cells in intestinal grafts, categorised by

634    time post-transplant (n=37; mean +/- SEM).

635    (D) Percentage of recipient-origin CD3+ T cells in intestinal grafts, categorised by

636    history of graft rejection. Unfilled circles, no rejection; Black, current rejection; Grey,

637    previous (post) rejection. (n=37; mean +/- SEM).

638    (E) Flow cytometry plot of HLA-A3 expression of graft-derived T cells in one subject

639    who demonstrated persistent donor chimerism in the intestinal graft 1865 days (5 years

640    and 1 month) post-transplant.

641    (F) Percentage of donor-origin CD3+ T cells in the blood of intestinal transplant

642    recipients, categorised by time post-transplant (n=14; mean +/- SEM). Dashed line at

643    4% represents the cut-off for significant macrochimerism from prior studies (Fu et al.,

644    2019; Zuber et al., 2015).

28

645    (G) Conventional CD8+ and CD4+ T cell subsets in the small intestinal graft as a

646    proportion of total T cells, categorised by time post-transplant (n=41; mean +/- SEM).

647    (H) The percentage of recipient-derived T cells infiltrating the intestinal graft within

648    conventional CD8+ and CD4+ T cell subsets, categorised by time post-transplant (n=41;

649    mean +/- SEM).

650    (I) Unconventional non-Vδ2+ γδ T cell, Vδ2+ γδ T cell, and Vα7.2+CD161+ CD8+ T

651    cell (mucosal-associated invariant T cells) subsets in the small intestinal graft as a

652    proportion of total T cells, categorised by time post-transplant (n=41; mean +/- SEM).

653    (J) The percentage of recipient-derived T cells infiltrating the intestinal graft within

654    unconventional non-Vδ2+ γδ T cell (n=27), Vδ2+ γδ T cell (n=25), and Vα7.2+CD161+

655    CD8+ T cell subsets (20), categorised by time post-transplant (mean +/- SEM).

656    (K) Representative flow cytometry plot of CD69 and CD103 expression on donor-

657    and recipient-derived CD8+ and CD4+ T cells in the intestinal graft.

658    (L) Percentage of donor- and recipient-derived CD8+ and CD4+ T cells in the

659    intestinal graft co-expressing CD69 and CD103 categorised by time post-transplant

660    (n=35; median marked with black line). Blue, CD69-103- cells; Red, CD69+CD103-

661    cells; Black, CD69+CD103+ cells.

662    For further analysis of surface marker expression, rare populations with fewer than

663    10 cells were excluded from the analysis (J, L). Statistical analysis performed with 1-

664    way ANOVA with Dunnett's multiple comparisons test. *, P ≤ 0.05; **, P ≤ 0.01.

665

666

667

668      Figure 2. **Transcriptionally distinct tissue resident memory (T<sub>RM</sub>) T cell**

669      **populations at single cell level, delineated by CD103 expression.**

670      (A) Schematic diagram of two scRNAseq experiments. Biopsies of small intestinal

671      transplant tissue were collected from subjects at endoscopy, then dissociated to isolate

672      intestinal lymphocytes. These were sorted by FACS, first with bulk sorting of donor-

673      derived T cells in Experiment 1, then with index sorting of donor-derived CD103- and

674      CD103+ T cells in Experiment 2, before scRNAseq library preparation and sequencing

675      using the 10x Genomics platform (Experiment 1) or the Smart-Seq2 protocol

676      (Experiment 2).

677      (B) tSNE plot of 974 donor-derived T cells from a single subject showing four

678      transcriptionally distinct populations of conventional CD4+ and CD8+ T cells.

679      (C) Dot plot of key gene identifiers for the four clusters showing two clusters of CD8+

680      T cells, and two clusters of CD4+ T cells, including one containing cells expressing

681      *IL2RA* and *FOXP3*, consistent with a regulatory T cell phenotype. Dot size indicates the

682      proportion of cells in which the gene is present. Colour intensity indicates the mean

683      expression level of the gene in cells in that cluster.

684      (D) Heatmap indicating hierarchical clustering of gene expression of CD8+ donor-

685      derived T cells from population 1 and population 2. Cell labels above indicate cluster:

686      Red, population 1; Blue, population 2. Genes of interest are highlighted.

687      (E) tSNE plot showing the expression of key genes upregulated in CD8+ population

688      2 (top row) or upregulated in CD8+ population 1 (bottom row).

689      (F) Dot plot showing the expression of 13 genes previously associated with tissue

690      residency in human CD69+ T cells (Kumar et al., 2017). Dot size indicates the

30

691    proportion of cells in which the gene is present. Colour intensity indicates the mean

692    level of expression of the gene in cells in that cluster.

693        (G) Hierarchical clustering and UMAP plot of 196 index-sorted CD103- and CD103+

694    CD8+ donor-derived T cells from two subjects identified three transcriptionally distinct

695    clusters of conventional CD8+ T cells. Cell labels below the dendrogram indicate the

696    plate used for sorting, the subject, and the CD103 expression determined by index

697    sorting. For UMAP plot: circles, CD103- cells by index-sorting; triangles, CD103+ cells

698    by index-sorting; square, unknown CD103 expression by index-sorting.

699        (H) Volcano plot of differential gene expression between cluster 1 and clusters 2 & 3

700    identified in (G), with genes upregulated (right) or down regulated (left) in clusters 2&3

701    compared to cluster 1. $\log_2$(fold change) is plotted against the FDR-adjusted p-value,

702    with horizontal dotted line at FDR=0.05. Differentially expressed genes are marked in

703    blue, with those differentially expressed both Experiments 1 and 2 marked in red.

704        (I) Correlation of $\log_2$(fold change) between populations 1 vs 2 from Experiment 1

705    (10x Genomics, x-axis) and clusters 2&3 vs cluster 1 from Experiment 2 (Smart-Seq2,

706    y-axis). Blue, genes differentially expressed in both experiments; green, genes

707    differentially expressed in Experiment 1 only; yellow, genes differentially expressed in

708    Experiment 2 only; grey, genes not differentially expressed. Genes shown were

709    expressed in both experiments.

710        (J) Venn diagram showing differentially expressed genes upregulated (red) or

711    downregulated (blue) in cluster 1 (CD103-) of Experiment 2 (Smart-Eeq2), or CD8+

712    population 2 of Experiment 1 (10x Genomics). A core gene set of 30 genes that

713    differentiated the two populations in both experiments are listed.

714

715

716    Figure 3. **Localisation and phenotype of CD103- and CD103+ intestinal T$_{RM}$**

717    **CD8+ populations.**

718    (A) Fluorescence microscopy chip cytometry image of small intestinal transplant

719    mucosa from a single subject 3 months post-transplant. The donor was HLA-A3+, and

720    recipient was HLA-A3-. False colour fluorescence imaging for cytokeratin (grey), CD3

721    (purple), CD8 (red), CD103 (blue), and HLA-A3 (green). Donor-derived CD8+ CD103+

722    and CD103- cells are indicated by white and yellow arrows respectively.

723    (B,C) Phenotypic analysis of CD8+ T cell populations in healthy small intestine.

724    (B) tSNE representation of CD8+ T cell phenotype from spectral flow cytometry

725    concatenated from 5 healthy control subjects, with expression of the following markers

726    superimposed: CD69 and CD103 (first row); CD161, CD7, CD127, β2-integrin,

727    granzyme K, KLRG1, and Ki-67 (second row). The location of cells co-expressing CD69

728    and CD103 is indicated. Blue, CD69-103- cells; Red, CD69+CD103- cells; Black,

729    CD69+CD103+ cells.

730    (C) Proportion of positive cells (CD161, KLRG1, Ki-67) or MFI (CD7, CD127, β2-

731    integrin, granzyme K) of CD8+ T cells, categorised by CD69 and CD103 expression, in

732    small intestinal biopsies from healthy control subjects (n=10). Mean percentage or MFI

733    represented by bars. Connecting lines represent populations from the same subject.

734    Blue, CD69-103- cells; Red, CD69+CD103- cells; Black, CD69+CD103+ cells.

735    (D-J) Phenotypic analysis of recipient-derived CD8+ T cell populations infiltrating the

736    intestinal transplant graft.

737    (D) The proportion of recipient-derived CD8+ T cells co-expressing CD69 and

738    CD103 in intestinal transplant grafts, categorised by time post-transplant (n=35). Blue,

739    CD69-103- cells; Red, CD69+CD103- cells; Black, CD69+CD103+ cells.

740    (E-I) Proportion of CD161+ cells (E), Ki-67+ cells (F) or MFI of CD127 (G), granzyme

741    K (H), and β2 integrin (I) of recipient-derived CD8+ T cells, categorised by CD69 and

742    CD103 expression and time post-transplant, in intestinal transplant grafts (n=23). Mean

743    percentage or MFI represented by bars. Black lines connect populations from the same

744    sample. Blue, CD69-103- cells; Red, CD69+CD103- cells; Black, CD69+CD103+ cells.

745    (J) Representative histogram of β2 integrin surface expression by circulating,

746    intestinal CD69-, intestinal CD69+CD103-, and intestinal CD69+CD103+ CD8+ T cells.

747    Statistical analysis performed with one-way ANOVA with Tukey's multiple

748    comparisons test. *, P ≤ 0.05; **, P ≤ 0.01; ***, P ≤ 0.001; ****, P ≤ 0.0001.

749

750

751    Figure 4. **Functional capacity of small intestinal CD8+ T cell populations.**

752    (A-D) Cytokine production by small intestinal CD8+ T cells.

753    Representative histograms of expression, and group summaries of proportion of

754    CD8+ T cells expressing TNFα (A), IFNγ (B), CCL4 (C), and IL-2 (D) after 4-hour

755    stimulation with PMA and ionomycin in the presence of brefeldin A and monensin,

756    categorised by CD69 and CD103 expression, in small intestinal biopsies from healthy

757    control subjects (n=10). Blue, CD69-103- cells; Red, CD69+CD103- cells; Black,

758    CD69+CD103+ cells.

759    (E) Mean proportion of CD8+ T cells expressing 0, 1, 2, 3, or 4 of the cytokines or

760     chemokines TNFα, IFNγ, CCL4, or IL-2, categorised by CD69 and CD103 co-

761     expression, from small intestinal biopsies from healthy control subjects (n=10).

762          (F) Mean percentage (+/- SEM) of CD8+ T cells co-expressing TNFα, IFNγ, CCL4,

763     or IL-2 production after PMA/ionomycin stimulation as described, categorised by CD69

764     and CD103 expression. Blue, CD69-103- cells; Red, CD69+CD103- cells; Black,

765     CD69+CD103+ cells.

766          Statistical analysis performed with one-way ANOVA with Tukey's multiple

767     comparisons test. *, P ≤ 0.05; **, P ≤ 0.01; ***, P ≤ 0.001.

768

769

770     Figure 5. **Phenotype and function of small intestinal CD4+ T cell populations.**

771          (A) MFI (CD161, CD7, CD127, β2-integrin, granzyme K, and KLRG1) or percentage

772     positive (Ki67) of CD4+ T cells, categorised by CD69 and CD103 expression, in small

773     intestinal biopsies from healthy control subjects (n=10). MFI represented by bars.

774     Connecting lines represent populations from the same subject. Blue, CD69-103- cells;

775     Red, CD69+CD103- cells; Black, CD69+CD103+ cells.

776          (B) MFI of β2-integrin of recipient-derived CD4+ T cells, categorised by CD69 and

777     CD103 expression and time post-transplant, in intestinal transplant grafts (n=21). MFI

778     represented by bars. Blue, CD69-103- cells; Red, CD69+CD103- cells; Black,

779     CD69+CD103+ cells.

780          (C-I) Cytokine production by small intestinal CD4+ T cells.

781          Representative histograms of expression, and group summaries of proportion of

782     CD4+ T cells expressing IL-17A (C), TNFα (D), IFNγ (E), IL-2 (F), CCL-4 (G), and IL-10

783   (H) after 4-hour stimulation with PMA and ionomycin in the presence of brefeldin A and

784   monensin, categorised by CD69 and CD103 expression, in small intestinal biopsies

785   from healthy control subjects (n=10). Blue, CD69-103- cells; Red, CD69+CD103- cells;

786   Black, CD69+CD103+ cells.

787      (I) Mean proportion of CD4+ T cells expressing 0, 1, 2, 3, 4, 5, or 6 of the cytokines

788   or chemokines IL-17A, TNFα, IFNγ, CCL4, IL-2, or IL-10, categorised by CD69 and

789   CD103 co-expression, from small intestinal biopsies from healthy control subjects

790   (n=10).

791      Statistical analysis performed with one-way ANOVA with Tukey's multiple

792   comparisons test. *, P ≤ 0.05; **, P ≤ 0.01; ***, P ≤ 0.001.

793

794

795   **Supplemental Figure 1.**

796      (A) Illustration demonstrating the principle of HLA allele congenic cell tracking to

797   identify donor- and recipient-derived T cell populations in the transplanted small

798   intestinal graft using fluorophore-conjugated antibodies to Class I HLA haplotypes

799   discordant between donor and recipient.

800      (B) Representative flow cytometry plot of Class I HLA non-specific staining (0.01-

801   0.12%) from a non-transplant PBMC sample. Gated on Live CD3+ T cells.

802      (C) Representative flow cytometry gating scheme for identification of T cell subsets.

803      (D) Representative histogram of CD161 expression of paired donor- and recipient-

804   derived CD8+ intestinal T cells.

805      (E) Percentage of CD161+ donor- and recipient-derived CD8+ intestinal T cells

806    categorised by time post-transplant (left), or grouped, with paired samples connected by

807    black lines (right) (n=15; mean +/- SEM).

808        Statistical analysis performed with Wilcoxon matched-pairs signed rank test. *, P ≤

809    0.05.

810

811

812    **Supplemental Figure 2:**

813        (A) Quality control parameters and thresholds for 10x Genomics scRNAseq

814    Experiment 1. Number of genes per cell (left), number of unique molecular identifiers

815    (UMIs) per cell (centre), and percentage of mitochondrial reads per cell (right) are

816    displayed. Each dot represents a single cell, with red and blue lines indicating maximum

817    and minimum thresholds, respectively.

818        (B) Dot plot showing expression in Experiment 1 of *ITGB2* and its potential

819    heterodimeric partner, *ITGAL* in Experiment 1. Other potential heterodimeric alpha

820    integrin partners, *ITGAD*, *ITGAM*, and *ITGAX* were not detected. Dot size indicates the

821    proportion of cells in which the gene is present. Colour intensity indicates the mean

822    expression level of the gene.

823        (C) Violin plots showing expression of *ITGB2* and its potential heterodimeric partner

824    *ITGAL* in Experiment 1. Other potential heterodimeric alpha integrin partners, *ITGAD*,

825    *ITGAM*, and *ITGAX* were not detected.

826

827        (D) Dot plot showing expression in Experiment 1 of 11 genes previously negatively

828    associated with tissue residency (downregulated in human CD69+ cells in comparison

829    to CD69- T cells; (Kumar et al., 2017)). Dot size indicates the proportion of cells in

830    which the gene is present. Colour intensity indicates the mean expression level of the

831    gene. Other genes in the geneset were not detected in the data (*SBK1*, *NPDC1*,

832    *KRT72*, *SOX13*, *KRT73*, *TSPAN18*, *PTGDS*).

833         (E) Violin plots showing expression in Experiment 1 of 11 genes previously

834    negatively associated with tissue residency (downregulated in human CD69+ cells in

835    comparison to CD69- T cells; (Kumar et al., 2017)).

836         (F) Violin plots showing expression in Experiment 1 of 13 genes previously

837    associated with tissue residency in human CD69+ T cells (Kumar et al., 2017),

838    demonstrating discordant expression in conventional T cell clusters.

839         (G-I) Quality control parameters and thresholds for Smart-Seq2 scRNAseq

840    Experiment 2.

841         (G) Histogram of number of reads per cell and (H) number of genes per cell. Red

842    and blue lines indicate maximum and minimum thresholds, respectively.

843         (I) Plot showing the percentage of External RNA Controls Consortium (ERCC) spike-

844    ins per cell against the number of genes per cell. Black line indicates upper threshold.

845         (J) Violin plots showing expression of *ITGB2* and its potential heterodimeric partners

846    *ITGAL* and *ITGAX* in Experiment 2. *ITGAD* and *ITGAM* were not detected in the data.

847

848    **Supplemental Figure 3.**

849         (A) Representative expression of CD161, CD7, CD127 (IL7R), ITGB2, and

850    Granzyme K on CD103- (red) and CD103+ (black) donor-derived T cells from the

851    intestinal transplant graft.

852     (B) The proportion of CD8+ T cells co-expressing CD69 and CD103 in small

853   intestinal biopsies from the duodenum (duo) or ileum from healthy control subjects (n=5

854   for both duodenum and ileum). Blue, CD69-103- cells; Red, CD69+CD103- cells; Black,

855   CD69+CD103+ cells.

856     (C) Representative flow cytometry gating of CD4+ CD25+CD127lo T cells.

857   Percentage of donor- or recipient-derived intestinal CD4+ CD25+CD127lo T cells.

858   Connecting lines represent populations from the same subject (n=23).

859

860

861

862

863 **References**

864 Adachi, T., T. Kobayashi, E. Sugihara, T. Yamada, K. Ikuta, S. Pittaluga, H. Saya, M.
865     Amagai, and K. Nagao. 2019. Hair follicle-derived IL-7 and IL-15 mediate skin-
866     resident memory T cell homeostasis and lymphoma. *Nature Medicine*. 1–10.
867     doi:10.1038/nm.3962.

868 Andrews, T.S., Andrews, T.S., and M. Hemberg. 2018. M3Drop: dropout-based feature
869     selection for scRNASeq. *Bioinformatics*. 35:2865–2867.
870     doi:10.1093/bioinformatics/bty1044.

871 Ariotti, S., M.A. Hogenbirk, F.E. Dijkgraaf, L.L. Visser, M.E. Hoekstra, J.-Y. Song, H.
872     Jacobs, J.B. Haanen, and T.N. Schumacher. 2014. T cell memory. Skin-resident
873     memory CD8+ T cells trigger a state of tissue-wide pathogen alert. *Science*.
874     346:101–105. doi:10.1126/science.1254803.

875 Bartolomé-Casado, R., O.J.B. Landsverk, S.K. Chauhan, L. Richter, D. Phung, V. Greiff,
876     L.F. Risnes, Y. Yao, R.S. Neumann, S. Yaqub, O. Øyen, R. Horneland, E.M.
877     Aandahl, V. Paulsen, L.M. Sollid, S.-W. Qiao, E.S. Bækkevold, and F.L. Jahnsen.
878     2019. Resident memory CD8 T cells persist for years in human small intestine. *J
879     Exp Med*. 157:jem.20190414–23. doi:10.1084/jem.20190414.

880 Bergsbaken, T., and M.J. Bevan. 2015. Proinflammatory microenvironments within the
881     intestine regulate the differentiation of tissue-resident CD8+ T cells responding to
882     infection. *Nat Immunol*. 16:406–414. doi:10.1038/ni.3108.

883    Beura, L.K., S. Wijeyesinghe, E.A. Thompson, M.G. Macchietto, P.C. Rosato, M.J.
884        Pierson, J.M. Schenkel, J.S. Mitchell, V. Vezys, B.T. Fife, S. Shen, and D.
885        Masopust. 2018. T Cells in Nonlymphoid Tissues Give Rise to Lymph- Node-
886        Resident Memory T Cells. *Immunity*. 48:327–338.e5.
887        doi:10.1016/j.immuni.2018.01.015.

888    Bolger, A.M., M. Lohse, and B. Usadel. 2014. Trimmomatic: a flexible trimmer for
889        Illumina sequence data. *Bioinformatics*. 30:2114–2120.
890        doi:10.1093/bioinformatics/btu170.

891    Boutet, M., L. Gauthier, M. Leclerc, G. Gros, V. de Montpreville, N. Théret, E.
892        Donnadieu, and F. Mami-Chouaib. 2016. TGFβ Signaling Intersects with CD103
893        Integrin Signaling to Promote T-Lymphocyte Accumulation and Antitumor Activity in
894        the Lung Tumor Microenvironment. *Cancer Res*. 76:1757–1769. doi:10.1158/0008-
895        5472.CAN-15-1545.

896    Butler, A., P. Hoffman, P. Smibert, E. Papalexi, and R. Satija. 2018. Integrating single-
897        cell transcriptomic data across different conditions, technologies, and species. *Nat
898        Biotechnol*. 36:411–420. doi:10.1038/nbt.4096.

899    de Leur, K., M. Dieterich, D.A. Hesselink, O.B.J. Corneth, F.J.M.F. Dor, G.N. Graav,
900        A.M.A. Peeters, A. Mulder, H.J.A.N. Kimenai, F.H.J. Claas, M.C.C.-V. Groningen,
901        L.J.W. Laan, R.W. Hendriks, and C.C. Baan. 2019. Characterization of donor and
902        recipient CD8+ tissue-resident memory T cells in transplant nephrectomies. *Sci
903        Rep*. 1–12. doi:10.1038/s41598-019-42401-9.

904    Dobin, A., C.A. Davis, F. Schlesinger, J. Drenkow, C. Zaleski, S. Jha, P. Batut, M.
905        Chaisson, and T.R. Gingeras. 2012. STAR: ultrafast universal RNA-seq aligner.
906        *Bioinformatics*. 29:15–21. doi:10.1093/bioinformatics/bts635.

907    Fagerholm, S.C., C. Guenther, M. Llort Asens, T. Savinko, and L.M. Uotila. 2019.
908        Beta2-Integrins and Interacting Proteins in Leukocyte Trafficking, Immune
909        Suppression, and Immunodeficiency Disease. *Front. Immunol.* 10:549–10.
910        doi:10.3389/fimmu.2019.00254.

911    Feau, S., R. Arens, S. Togher, and S.P. Schoenberger. 2011. Autocrine IL-2 is required
912        for secondary population expansion of CD8+ memory T cells. *Nat Immunol*. 12:908–
913        913. doi:10.1038/ni.2079.

914    Fergusson, J.R., M.H.H.U. hn, L. Swadling, L.J. Walker, A. Kurioka, A. Llibre, A.
915        Bertoletti, G.H.A. nder, E.W. Newell, M.M. Davis, E.S.-E.O. m, F. Powrie, S.
916        Capone, A. Folgori, E. Barnes, C.B. Willberg, J.E. Ussher, and P. Klenerman. 2015.
917        CD161intCD8+ T cells: a novel population of highly functional, memory CD8+ T
918        cells enriched within the gut. 1–13. doi:10.1038/mi.2015.69.

919    Fu, J., J. Zuber, M. Martinez, B. Shonts, A. Obradovic, H. Wang, S.-P. Lau, A. Xia, E.E.
920        Waffarn, K. Frangaj, T.M. Savage, M.T. Simpson, S. Yang, X.V. Guo, M. Miron, T.
921        Senda, K. Rogers, A. Rahman, S.-H. Ho, Y. Shen, A. Griesemer, D.L. Farber, T.

Kato, and M. Sykes. 2019. Human Intestinal Allografts Contain Functional Hematopoietic Stem and Progenitor Cells that Are Maintained by a Circulating Pool. *Stem Cell*. 24:227–239.e8. doi:10.1016/j.stem.2018.11.007.

Gebhardt, T., P.G. Whitney, A. Zaid, L.K. Mackay, A.G. Brooks, W.R. Heath, F.R. Carbone, and S.N. Mueller. 2011. Different patterns of peripheral migration by memory CD4+ and CD8+ T cells. *Nature*. 477:216–219. doi:10.1038/nature10339.

Gutierrez-Arcelus, M., N. Teslovich, A.R. Mola, R.B. Polidoro, A. Nathan, H. Kim, S. Hannes, K. Slowikowski, G.F.M. Watts, I. Korsunsky, M.B. Brenner, S. Raychaudhuri, and P.J. Brennan. 2019. Lymphocyte innateness defined by transcriptional states reflects a balance between proliferation and effector functions. *Nature Communications*. 1–15. doi:10.1038/s41467-019-08604-4.

Harris, R.A., D. Nagy-Szakal, S.A. Mir, E. Frank, R. Szigeti, J.L. Kaplan, J. Bronsky, A. Opekun, G.D. Ferry, H. Winter, and R. Kellermayer. 2014. DNA methylation-associated colonic mucosal immune and defense responses in treatment-naïve pediatric ulcerative colitis. *Epigenetics*. 9:1131–1137. doi:10.4161/epi.29446.

Hennig, C., N. Adams, and G. Hansen. 2009. A versatile platform for comprehensive chip-based explorative cytometry. *Cytometry*. 75A:362–370. doi:10.1002/cyto.a.20668.

Hombrink, P., C. Helbig, R.A. Backer, B. Piet, A.E. Oja, R. Stark, G. Brasser, A. Jongejan, R.E. Jonkers, B. Nota, O. Basak, H.C. Clevers, P.D. Moerland, D. Amsen, and R.A.W. van Lier. 2016. Programs for the persistence, vigilance and control of human CD8+ lung-resident memory T cells. *Nat Immunol*. 17:1467–1478. doi:10.1038/ni.3589.

Kennedy, N.A., A.T. Adams, R. Kalla, S. Heath, K.R.O.A. Leary, H. Drummond, D.C. Wilson, I.G. Gut, E.R. Nimmo, J. Satsangi, G. Lauc, H. Campbell, D.P.B. McGovern, V. Annese, V.Z. scaron, I.K. Permberton, M. Wuhrer, D. Kolarich, D.L. Fernandes, E. Theorodorou, V. Merrick, D.I. Spencer, R.A. Gardner, R. Doran, A. Shubhakar, R. Boyapati, I. Rudan, P. Lionetti, I.T.C.A.C.I. cacute, J.K.S.T. cacute, F.V.C.K. cacute, J.S. tambuk, M. Novokmet, M.P.C.I.C.B. cacute, O. Gornik, A. Andriulli, L. Cantoro, G. Sturniolo, G. Fiorino, N. Manetti, A. Latiano, A. Kohn, R.D.R.I. agrave, S. Danese, I.D. Arnott, C.L. Noble, C.W. Lees, A.G. Shand, G.-T. Ho, M.G. Dunlop, L. Murphy, J. Gibson, L. Evenden, N. Wrobel, T. Gilchrist, A. Fawkes, G.S.M. Kammeijer, F. Clerc, N. de Haan, A. Vojta, I.S.Z. ija, D. Markulin, M.K. cacute, P.D. cacute, Y. Aulchenko, T. van den Heuve, D. Jonkers, M. Pierik, S. Vatn, P. Ricanek, J.O.R. Jahnsen, P. You, J.S.O. Ivernes, A.B. Frengen, T.M.T.A. s, A.E.F. Moen, F.A. Dahl, J.C.L.O. m, G.S. Ekeland, T.E. Detlie, A.S.V. Keita, J.D.S.O. derholm, H. Hjortswang, J. Halfvarson, D. Bergemalm, F.G.O. n, M.D.A. Amato, L.T.O. rkvist, F. Hjelm, M. Gullberg, N. Nordberg, A. Ocklind, E. Pettersson, D. Ekman, M. Sundell, E. Modig, A.C.E.M. Veillard, R. Schoemans, et al. 2016. Integrative epigenome-wide analysis demonstrates that DNA methylation may mediate genetic risk in inflammatory bowel disease. *Nature Communications*. 7:1–14.

963      doi:10.1038/ncomms13507.

964   Kiselev, V.Y., K. Kirschner, M.T. Schaub, T. Andrews, A. Yiu, T. Chandra, K.N.
965        Natarajan, W. Reik, M. Barahona, A.R. Green, and M. Hemberg. 2017. SC3:
966        consensus clustering of single-cell RNA-seq data. *Nat Meth*. 14:483–486.
967        doi:10.1038/nmeth.4236.

968   Konnikova, L., G. Boschetti, A. Rahman, V. Mitsialis, J. Lord, C. Richmond, V.T. Tomov,
969        W. Gordon, S. Jelinsky, J. Canavan, A. Liss, S. Wall, M. Field, F. Zhou, J.D.
970        Goldsmith, M. Bewtra, D.T. Breault, M. Merad, and S.B. Snapper. 2018. High-
971        dimensional immune phenotyping and transcriptional analyses reveal robust
972        recovery of viable human immune and epithelial cells from frozen gastrointestinal
973        tissue. *Mucosal Immunology*. 1–10. doi:10.1038/s41385-018-0047-y.

974   Kumar, B.V., W. Ma, M. Miron, T. Granot, R.S. Guyer, D.J. Carpenter, T. Senda, X.
975        Sun, S.-H. Ho, H. Lerner, A.L. Friedman, Y. Shen, and D.L. Farber. 2017. Human
976        Tissue-Resident Memory T Cells Are Defined by Core Transcriptional and
977        Functional Signatures in Lymphoid and Mucosal Sites. *CellReports*. 20:2921–2934.
978        doi:10.1016/j.celrep.2017.08.078.

979   Leng, T., H.D. Akther, C.-P. Hackstein, K. Powell, T. King, M. Friedrich, Z.
980        Christoforidou, S. McCuaig, M. Neyazi, C.V. Arancibia-Cárcamo, J. Hagel, F.
981        Powrie, R.S. Peres, V. Millar, D. Ebner, R. Lamichhane, J. Ussher, T.S.C. Hinks, E.
982        Marchi, C. Willberg, P. Klenerman, and O.I. Investigators3. 2019. TCR and
983        Inflammatory Signals Tune Human MAIT Cells to Exert Specific Tissue Repair and
984        Effector Functions. *CellReports*. 28:3077–3091.e5.
985        doi:10.1016/j.celrep.2019.08.050.

986   Li, H., Li, H., B. Handsaker, B. Handsaker, A. Wysoker, A. Wysoker, T. Fennell, T.
987        Fennell, J. Ruan, J. Ruan, N. Homer, N. Homer, G. Marth, G. Marth, G. Abecasis,
988        G. Abecasis, R. Durbin, R. Durbin, and 1000 Genome Project Data Processing
989        Subgroup. 2009. The Sequence Alignment/Map format and SAMtools.
990        *Bioinformatics*. 25:2078–2079. doi:10.1093/bioinformatics/btp352.

991   Liao, Y., Liao, Y., G.K. Smyth, G.K. Smyth, W. Shi, and W. Shi. 2014. featureCounts: an
992        efficient general purpose program for assigning sequence reads to genomic
993        features. *Bioinformatics*. 30:923–930. doi:10.1093/bioinformatics/btt656.

994   Liu, D., Y.T. Bryceson, T. Meckel, G. Vasiliver-Shamis, M.L. Dustin, and E.O. Long.
995        2009. Integrin-Dependent Organization and Bidirectional Vesicular Traffic at
996        Cytotoxic Immune Synapses. *Immunity*. 31:99–109.
997        doi:10.1016/j.immuni.2009.05.009.

998   Lun, A.T.L., D.J. McCarthy, and J.C. Marioni. 2016. A step-by-step workflow for low-
999        level analysis of single-cell RNA-seq data with Bioconductor. *F1000Res*. 5:2122.
1000       doi:10.12688/f1000research.9501.2.

1001  Mackay, L.K., and A. Kallies. 2017. Transcriptional Regulation of Tissue-Resident

Lymphocytes. *Trends in Immunology*. 38:94–103. doi:10.1016/j.it.2016.11.004.

Mackay, L.K., M. Minnich, N.A.M. Kragten, Y. Liao, B. Nota, C. Seillet, A. Zaid, K. Man, S. Preston, D. Freestone, A. Braun, E. Wynne-Jones, F.M. Behr, R. Stark, D.G. Pellicci, D.I. Godfrey, G.T. Belz, M. Pellegrini, T. Gebhardt, M. Busslinger, W. Shi, F.R. Carbone, R.A.W. van Lier, A. Kallies, and K.P.J.M. van Gisbergen. 2016. Hobit and Blimp1 instruct a universal transcriptional program of tissue residency in lymphocytes. *Science*. 352:459–459. doi:10.1126/science.aad2035.

Mayassi, T., K. Ladell, H. Gudjonson, J.E. McLaren, D.G. Shaw, M.T. Tran, J.J. Rokicka, I. Lawrence, J.-C. Grenier, V. van Unen, C. Ciszewski, M. Dimaano, H.E. Sayegh, V. Kumar, C. Wijmenga, P.H.R. Green, R. Gokhale, H. Jericho, C.E. Semrad, S. Guandalini, A.R. Dinner, S.S. Kupfer, H.H. Reid, L.B. Barreiro, J. Rossjohn, D.A. Price, and B. Jabri. 2019. Chronic Inflammation Permanently Reshapes Tissue-Resident Immunity in Celiac Disease. *Cell*. 1–35. doi:10.1016/j.cell.2018.12.039.

McCarthy, D.J., K.R. Campbell, A.T.L. Lun, and Q.F. Wills. 2017. Scater: pre-processing, quality control, normalization and visualization of single-cell RNA-seq data in R. *Bioinformatics*. 247:btw777–1186. doi:10.1093/bioinformatics/btw777.

McInnes, L., J. Healy, and J. Melville. 2018. UMAP: Uniform Manifold Approximation and Projection for Dimension Reduction. arXiv preprint arXiv:1802.03426

McNamara, H.A., Y. Cai, M.V. Wagle, Y. Sontani, C.M. Roots, L.A. Miosge, J.H. O'Connor, H.J. Sutton, V.V. Ganusov, W.R. Heath, P. Bertolino, C.G. Goodnow, I.A. Parish, A. Enders, and I.A. Cockburn. 2017. Up-regulation of LFA-1 allows liver-resident memory T cells to patrol and remain in the hepatic sinusoids. *Science Immunology*. 2:1–11. doi:10.1126/sciimmunol.aaj1996.

Miao, Z., K. Deng, X. Wang, and X. Zhang. 2018. DEsingle for detecting three types of differential expression in single-cell RNA-seq data. *Bioinformatics*. 34:3223–3224. doi:10.1093/bioinformatics/bty332.

Oja, A.E., B. Piet, C. Helbig, R. Stark, D. van der Zwan, H. Blaauwgeers, E.B.M. Remmerswaal, D. Amsen, R.E. Jonkers, P.D. Moerland, M.A. Nolte, R.A.W. van Lier, and P. Hombrink. 2017. Trigger-happy resident memory CD4+ T cells inhabit the human lungs. *Mucosal Immunology*. 11:654–667. doi:10.1038/mi.2017.94.

Pallett, L.J., J. Davies, E.J. Colbeck, F. Robertson, N. Hansi, N.J.W. Easom, A.R. Burton, K.A. Stegmann, A. Schurich, L. Swadling, U.S. Gill, V. Male, T. Luong, A. Gander, B.R. Davidson, P.T.F. Kennedy, and M.K. Maini. 2017. IL-2high tissue-resident T cells in the human liver: Sentinels for hepatotropic infection. *J Exp Med*. 214:1567–1580. doi:10.1084/jem.20162115.

Park, S.L., T. Gebhardt, and L.K. Mackay. 2019. Tissue-Resident Memory T Cells in Cancer Immunosurveillance. *Trends in Immunology*. 1–13. doi:10.1016/j.it.2019.06.002.

1041  Picelli, S., Å.K. Björklund, O.R. Faridani, S. Sagasser, G. Winberg, and R. Sandberg.
1042      2013. Smart-seq2 for sensitive full-length transcriptome profiling in single cells. *Nat*
1043      *Meth*. 10:1096–1098. doi:10.1038/nmeth.2639.

1044  Picelli, S., O.R. Faridani, A.S.K.B.O. rklund, G.O.S. Winberg, S. Sagasser, and R.
1045      Sandberg. 2014. Full-length RNA-seq from single cells using Smart-seq2. *Nat*
1046      *Protoc*. 9:171–181. doi:10.1038/nprot.2014.006.

1047  Provine, N.M., B. Binder, M.E.B. FitzPatrick, A. Schuch, L.C. Garner, K.D. Williamson,
1048      B. van Wilgenburg, R. Thimme, P. Klenerman, and M. Hofmann. 2018. Unique and
1049      Common Features of Innate-Like Human Vδ2+ γδT Cells and Mucosal-Associated
1050      Invariant T Cells. *Front. Immunol.* 9:120–12. doi:10.3389/fimmu.2018.00756.

1051  Raeber, M.E., Y. Zurbuchen, D. Impellizzieri, and O. Boyman. 2018. The role of
1052      cytokines in T-cell memory in health and disease. *Immunol Rev*. 283:176–193.
1053      doi:10.1111/imr.12644.

1054  Román, J., N. Planell, J.J. Lozano, M. Aceituno, M. Esteller, C. Pontes, D. Balsa, M.
1055      Merlos, J. Panés, and A. Salas. 2013. Evaluation of Responsive Gene Expression
1056      as a Sensitive and Specific Biomarker in Patients with Ulcerative Colitis. *Inflamm*
1057      *Bowel Dis*. 19:221–229. doi:10.1002/ibd.23020.

1058  Sancho, D., M. Gómez, and F. Sánchez-Madrid. 2005. CD69 is an immunoregulatory
1059      molecule induced following activation. *Trends in Immunology*. 26:136–140.
1060      doi:10.1016/j.it.2004.12.006.

1061  Schenkel, J.M., K.A. Fraser, L.K. Beura, K.E. Pauken, V. Vezys, and D. Masopust.
1062      2014. Resident memory CD8 T cells trigger protective innate and adaptive immune
1063      responses. *Science*. 346:98–101. doi:10.1126/science.1254536.

1064  Shiow, L.R., D.B. Rosen, N. Brdičková, Y. Xu, J. An, L.L. Lanier, J.G. Cyster, and M.
1065      Matloubian. 2006. CD69 acts downstream of interferon-α/β to inhibit S1P1 and
1066      lymphocyte egress from lymphoid organs. *Nature*. 440:540–544.
1067      doi:10.1038/nature04606.

1068  Snyder, M.E., M.O. Finlayson, T.J. Connors, P. Dogra, T. Senda, E. Bush, D.
1069      Carpenter, C. Marboe, L. Benvenuto, L. Shah, H. Robbins, J.L. Hook, M. Sykes, F.
1070      D'Ovidio, M. Bacchetta, J.R. Sonett, D.J. Lederer, S. Arcasoy, P.A. Sims, and D.L.
1071      Farber. 2019. Generation and persistence of human tissue-resident memory T cells
1072      in lung transplantation. *Science Immunology*. 4:1–17.

1073  Stuart, T., A. Butler, P. Hoffman, C. Hafemeister, E. Papalexi, W.M. Mauck, W.M.
1074      Mauck III, Y. Hao, M. Stoeckius, P. Smibert, and R. Satija. 2019. Comprehensive
1075      Integration of Single-Cell Data. *Cell*. 177:1888–1902.e21.
1076      doi:10.1016/j.cell.2019.05.031.

1077  Szabo, P.A., M. Miron, and D.L. Farber. 2019. Location, location, location: Tissue
1078      resident memory T cells in mice and humans. *Science Immunology*. 4:1–12.

1079  doi:10.1126/sciimmunol.aas9673.

1080 Thome, J.J.C., N. Yudanin, Y. Ohmura, M. Kubota, B. Grinshpun, T. Sathaliyawala, T.
1081  Kato, H. Lerner, Y. Shen, and D.L. Farber. 2014. Spatial Map of Human T Cell
1082  Compartmentalization and Maintenance over Decades of Life. *Cell*. 159:814–828.
1083  doi:10.1016/j.cell.2014.10.026.

1084 Verma, N.K., E. Dempsey, A. Long, A. Davies, S.P. Barry, P.G. Fallon, Y. Volkov, and
1085  D. Kelleher. 2012. Leukocyte Function-associated Antigen-1/Intercellular Adhesion
1086  Molecule-1 Interaction Induces a Novel Genetic Signature Resulting in T-cells
1087  Refractory to Transforming Growth Factor-β Signaling. *Journal of Biological*
1088  *Chemistry*. 287:27204–27216. doi:10.1074/jbc.M112.376616.

1089 Walsh, D.A., H. Borges da Silva, L.K. Beura, C. Peng, S.E. Hamilton, D. Masopust, and
1090  S.C. Jameson. 2019. The Functional Requirement for CD69 in Establishment of
1091  Resident Memory CD8 +T Cells Varies with Tissue Location. *J.I.* 203:946–955.
1092  doi:10.4049/jimmunol.1900052.

1093 Zimmerli, S.C., A. Harari, C. Cellerai, F. Vallelian, P.-A. Bart, and G. Pantaleo. 2005.
1094  HIV-1-specific IFN-γ/IL-2-secreting CD8 T cells support CD4-independent
1095  proliferation of HIV-1-specific CD8 T cells. *Proc. Natl. Acad. Sci. U.S.A.* 102:7239–6.
1096  doi:10.1073/pnas.0502393102.

1097 Zuber, J., B. Shonts, S.P. Lau, A. Obradovic, J. Fu, S. Yang, M. Lambert, S. Coley, J.
1098  Weiner, J. Thome, S. DeWolf, D.L. Farber, Y. Shen, S. Caillat-Zucman, G. Bhagat,
1099  A. Griesemer, M. Martinez, T. Kato, and M. Sykes. 2016. Bidirectional intragraft
1100  alloreactivity drives the repopulation of human intestinal allografts and correlates
1101  with clinical outcome. *Science Immunology*. 1:eaah3732–eaah3732.
1102  doi:10.1126/sciimmunol.aah3732.

1103 Zuber, J., S. Rosen, B. Shonts, B. Sprangers, T.M. Savage, S. Richman, S. Yang, S.P.
1104  Lau, S. DeWolf, D. Farber, G. Vlad, E. Zorn, W. Wong, J. Emond, B. Levin, M.
1105  Martinez, T. Kato, and M. Sykes. 2015. Macrochimerism in Intestinal
1106  Transplantation: Association With Lower Rejection Rates and Multivisceral
1107  Transplants, Without GVHD. *American Journal of Transplantation*. 15:2691–2703.
1108  doi:10.1111/ajt.13325.

1109 Zundler, S., E. Becker, M. Spocinska, M. Slawik, L. Parga-Vidal, R. Stark, M. Wiendl, R.
1110  Atreya, T. Rath, M. Leppkes, K. Hildner, R.X.O.L.X. pez-Posadas, S.X.R. Lukassen,
1111  A.B. Ekici, C. Neufert, I. Atreya, K.P.J.M. Gisbergen, and M.F. Neurath. 2019. Hobit-
1112  and Blimp-1-driven CD4+ tissue-resident memory T cells control chronic intestinal
1113  inflammation. *Nature Immunology. 20:*288-300. doi:10.1038/s41590-018-0298-5.
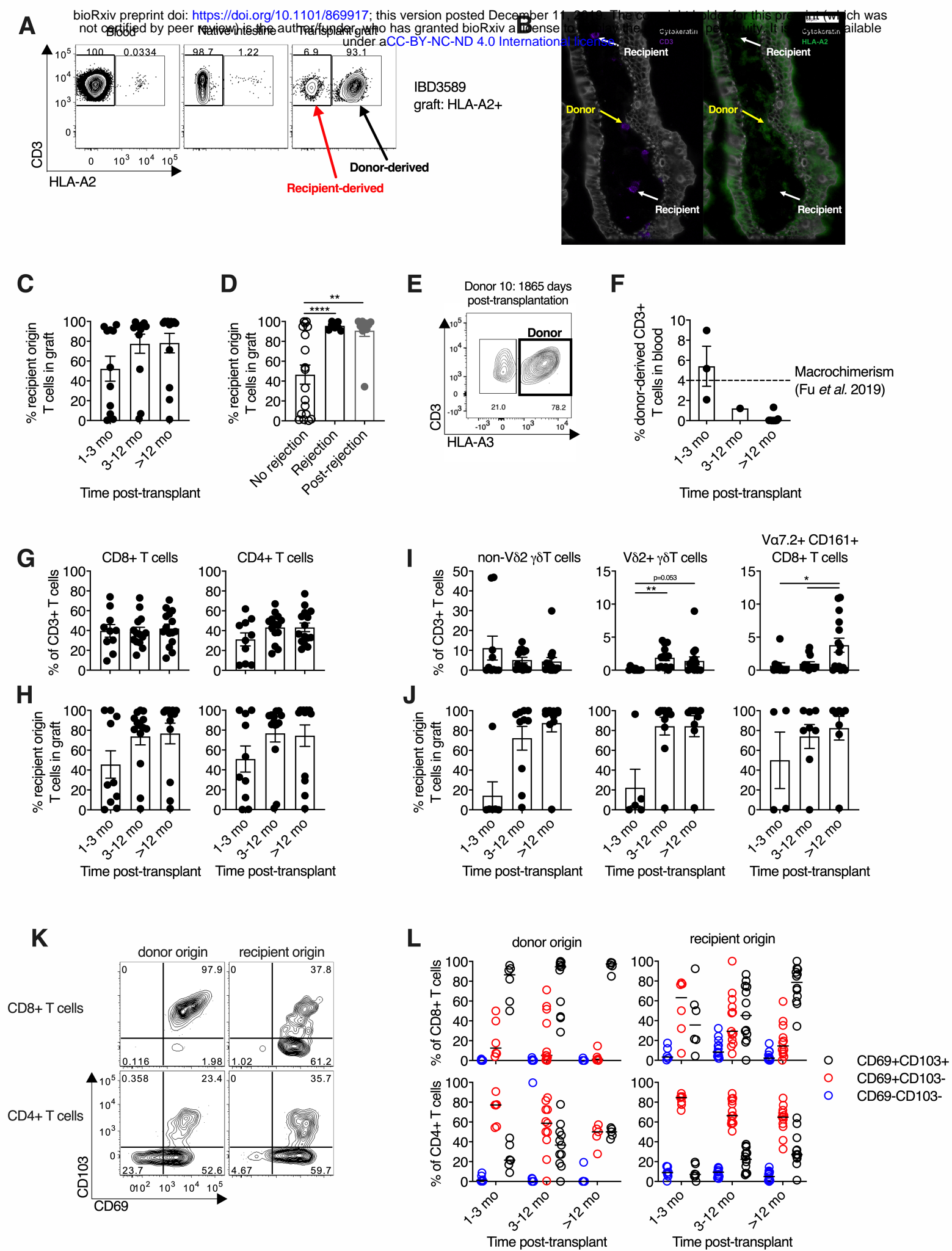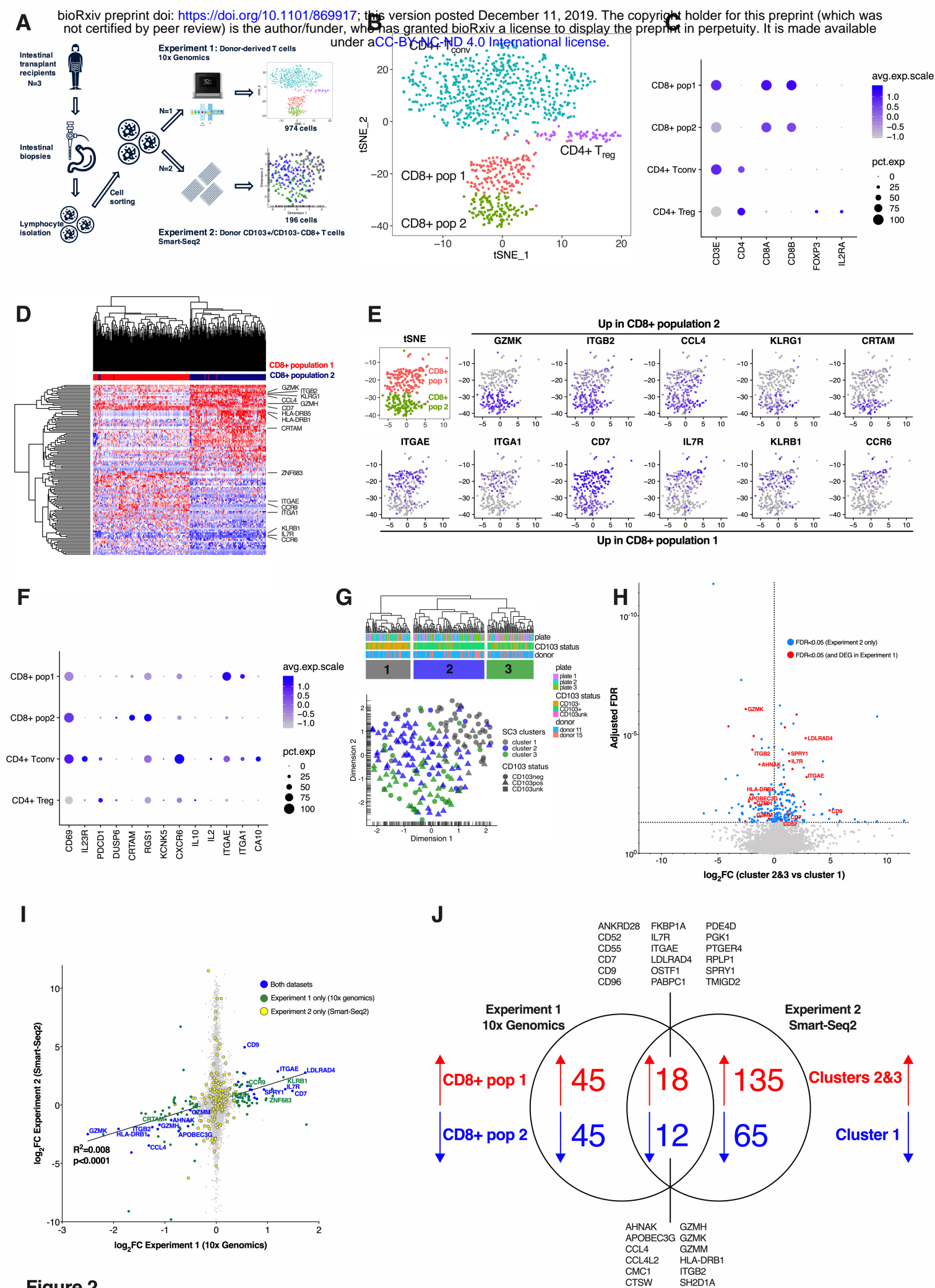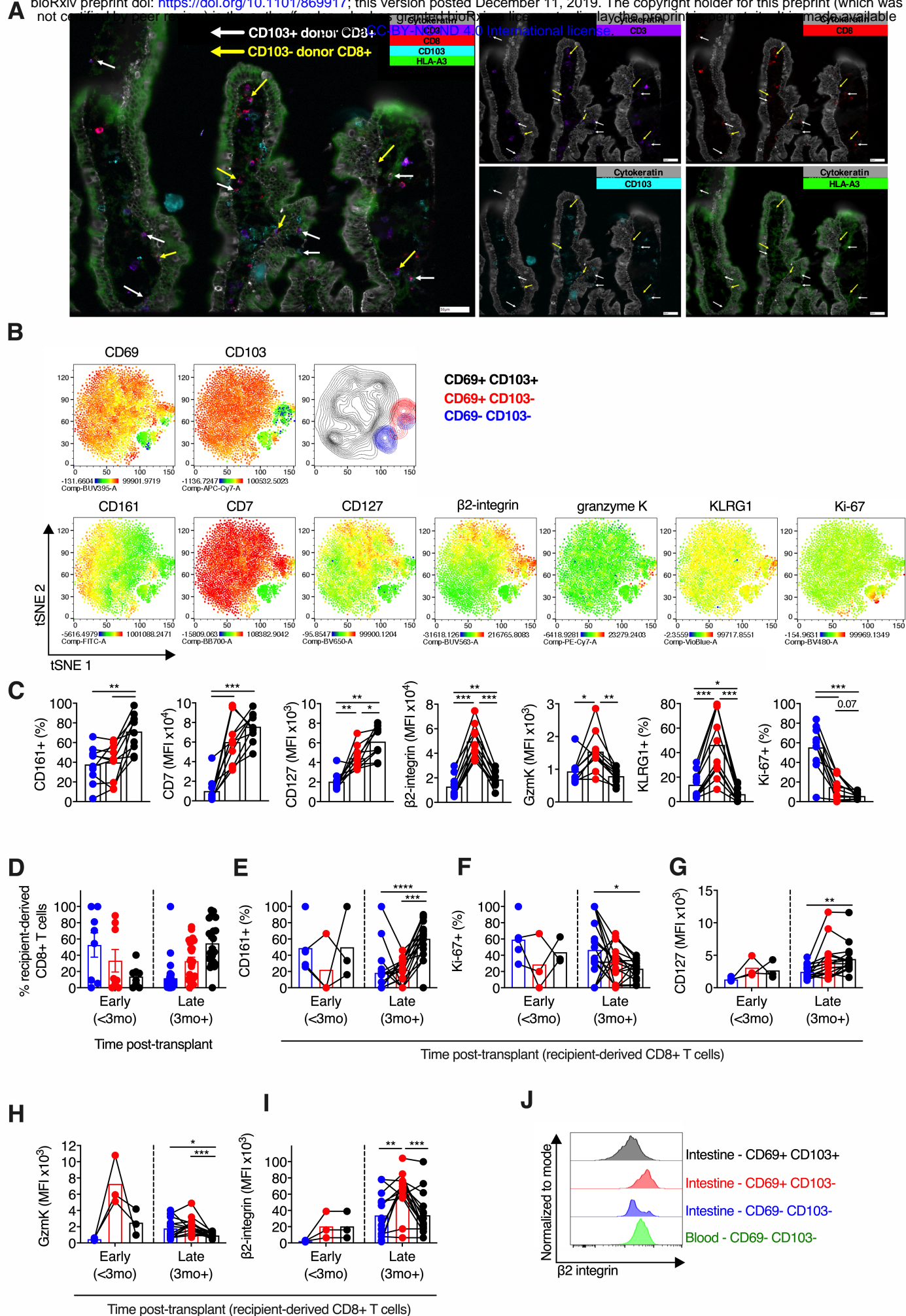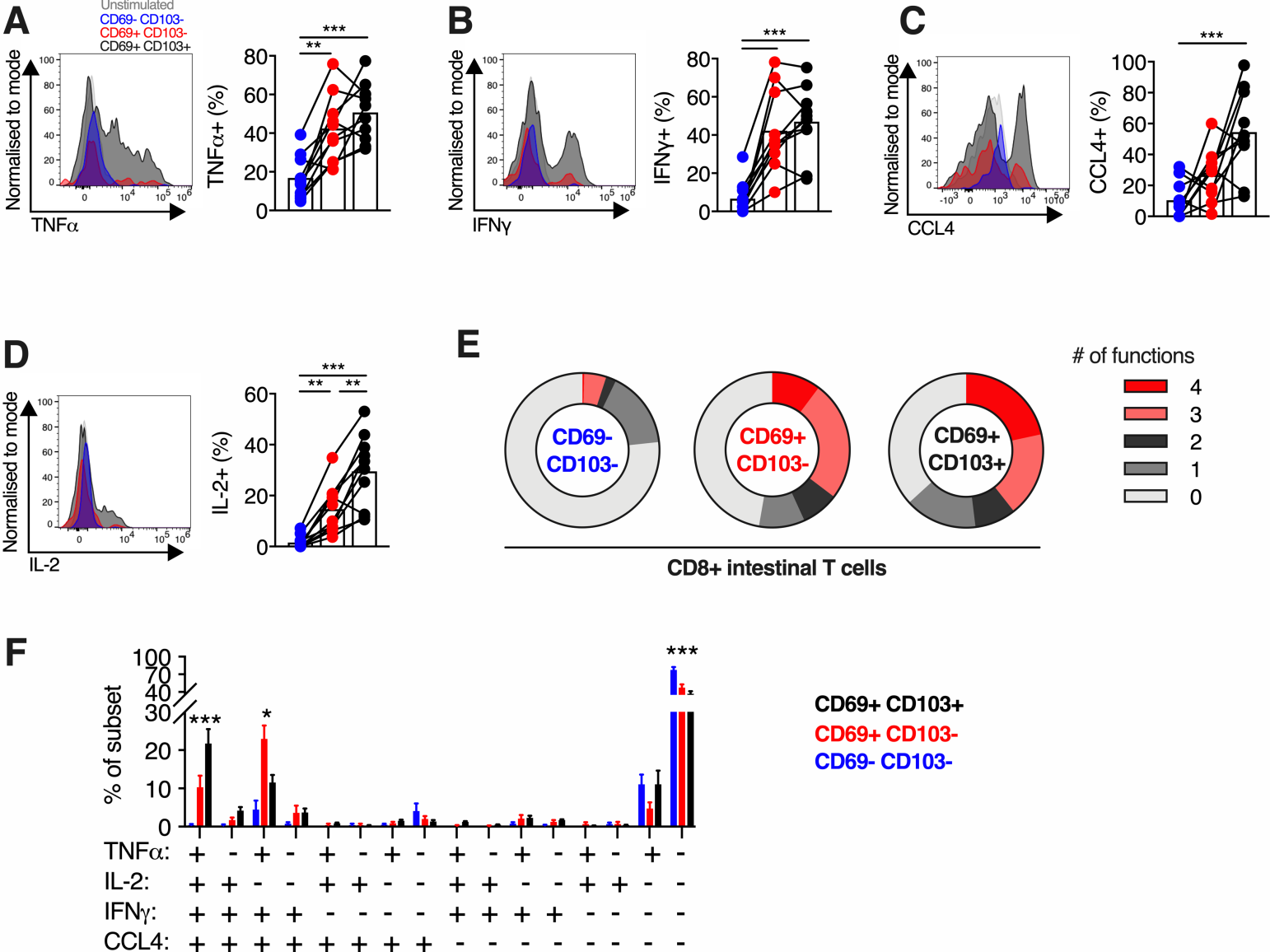
1114

Figure 1

**Figure 2**

**Figure 3**

**Figure 4**

**Figure 5**